

Spectroscopic study of the variability of three northern Of⁺ supergiants

M. De Becker¹, G. Rauw and N. Linder

Institut d'Astrophysique et de Géophysique, Université de Liège, 17, Allée du 6 Août, B5c,
B-4000 Sart Tilman, Belgium

debecker@astro.ulg.ac.be

Received _____; accepted _____

Based on observations collected at the Observatoire de Haute-Provence (France).

¹Postdoctoral Researcher FRS/FNRS (Belgium)

ABSTRACT

The transition from early Of stars to WN type objects is poorly understood. O-type supergiants with emission lines (OIf⁺) are considered to be intermediate between these two classes. The scope of this paper is to investigate the spectral variability of three Of⁺ supergiants. We constituted spectral time series of unprecedented quality for our targets (~ 200 spectra in total), essentially in the blue domain, covering time-scales from a few hours up to a few years. Time Variance Spectrum (TVS) and Fourier analyses were performed in order to characterize their spectral variability. We report on a correlated significant line profile variability in the prominent He II λ 4686 and H β lines most likely related to the strong stellar winds. The variability pattern is similar for the three stars investigated (HD 14947, HD 15570 and HD 16691), and the main differences are more quantitative than qualitative. However, the reported time-scales are somewhat different, and the most striking variability pattern is reported for HD 16691. We did not find any clear evidence for binarity, and we focus mainly on an interpretation based on a single star scenario. We show that the behaviour of the three stars investigated in this study present strong similarities, pointing to a putative common scenario, even though a few differences should be noted. Our preferred interpretation scheme is that of Large Scale Corotating Structures modulating the profile of the lines that are produced in the strong stellar wind.

Subject headings: stars: early-type – stars: mass-loss – stars: supergiants – stars: individual: HD 14947 – stars: individual: HD 15570 – stars: individual: HD 16691

1. Introduction

In the standard evolutionary scheme, Of stars are the progenitors of Wolf-Rayet stars. As the star evolves into the supergiant phase, its stellar wind becomes stronger, which translates in some lines appearing in strong emission in the optical spectrum (He II λ 4686, H α ...). On the other hand, WR stars are characterized by strong emission lines, also related to their strong and dense winds. The similarities in the spectral morphology in the optical domain of these two classes of stars is a well-established fact for several decades (Conti 1976). In this context, Conti et al. (1995) discussed the similarities between the K-band spectra of the O4If⁺ stars HD 16691 and HD 190429A, and those of Wolf-Rayet stars. The latter authors pointed out the *connection in the spectral morphology between some early Of and WN stars* likely attributable to an evolutionary relationship. Another star worth considering in the same framework is the bright O4If⁺ star HD 15570, member of the open cluster IC 1805, that has been qualified as transitional by Willis & Stickland (1980) on the basis of its UV spectral properties. In addition, Cappa & Herbstmeier (2000) reported on the probable presence around HD 16691 and HD 14947 (O5If⁺) of interstellar bubbles that are very similar in shape to other bubbles surrounding WR stars.

If one wants to address the issue of the dynamics of the quite extreme stellar winds of such transitional objects, variability studies are likely to bring crucial information. In their study of the line profile variations of H α , Markova et al. (2005) reported on significant variations in the case of HD 190429A, HD 14947 and HD 16691. Even though their time series were limited to only a few spectra, they pointed out some similarities in the spectral shape and in the behaviour of these stars. They also noted that the lack of significant line profile variability in other lines such as He II λ 6527 Å suggests that the variations in H α were probably due to processes in the wind. However, to investigate in detail such a line profile variability, a very good time sampling is required.

In the context of the present study, we focus on three targets: HD 14947, HD 16691 and HD 15570. The latter one has already been investigated by De Becker & Rauw (2005), but the time series was not well suited for the study of short time scale variations, i.e. of the order of the day or shorter. The significantly improved time series presented here are used to more adequately characterize the line profile variability of our three targets. We first discuss the optical spectrum of the stars (Section 3). The main part of the paper consists in a detailed description of the variability study (Section 4), followed by a discussion in Section 5. Our conclusions are presented in Section 6.

2. Observations and data reduction

Spectroscopic observations were collected at the Observatoire de Haute-Provence (OHP, France) during several observing runs from October 2004 to Autumn 2007. All spectra were obtained with the Aurélie spectrograph fed by the 1.52 m telescope (Gillet et al. 1994), using the same setup as described for instance by De Becker et al. (2004, 2006). Our collection of spectra is described in Table 1, and the detailed journal of the observations is given in Table 2. The typical exposure time was about 30 – 45 minutes, depending on the weather conditions. In order to carry out a detailed variability study of our targets, we organized the observing campaign in such a way that we covered time scales from a few hours up to a few years. In total, we obtained 57, 64 and 64 blue spectra between 4450 and 4900 Å respectively for HD 14947, HD 15570 and HD 16691. In addition, in October 2005, we obtained 7, 5 and 6 red spectra between 6340 and 6780 Å respectively for the three targets spread over a few days. The resolving power is about 8000 in the blue, and 11000 in the red. All data were treated following the reduction procedure already described by Rauw & De Becker (2004).

During this campaign, particular efforts were devoted to the sampling of many

Table 1: Description of observing runs for the blue domain. The first and second columns give the name of the campaign as used in the text as well as the instrumentation used. For each star, the next columns yield the number of spectra obtained, the time elapsed between the first and the last spectrum of the run (ΔT), the natural width ($\Delta\nu_{\text{nat}}$) of a peak of the power spectrum taken as $1/\Delta T$, and finally the mean signal-to-noise ratio of each data set. In the case of HD 15570, the information concerning observations before 2007 can be found in De Becker et al. (2006).

Obs. run	N	ΔT (d)	$\Delta\nu_{\text{nat}}$ (d ⁻¹)	S/N
<hr/> <hr/> HD 14947 <hr/>				
Oct.2004	4	10.1	0.99	360
Oct.2005	4	6.0	0.17	320
Sept.2006	2	2.0	0.50	290
Oct.2006	5	1.2	0.85	270
Aut.2007	42	26.1	0.04	300
<hr/> <hr/> HD 15570 <hr/>				
Aut.2007	28	11.0	0.09	300
<hr/> <hr/> HD 16691 <hr/>				
Oct.2004	5	10.0	0.10	300
Oct.2005	4	6.0	0.17	270
Sept.2006	2	4.0	0.25	210
Oct.2006	7	1.2	0.85	200
Aut.2007	46	26.0	0.04	300

time-scales. As this is a critical issue in variability studies, we managed to collect as much data as possible with various time intervals between two consecutive observations. Table 2 shows that the campaign spreads over more than three years for HD 14947 and HD 16691, and more than 7 years in the case of HD 15570, with several observing runs in between. Moreover, our targets were observed several times a night, over several nights, in order to cover shorter time-scales. We note that this observing campaign ended in October-November 2007, with a 28 consecutive nights of observation. The latter observing run allowed us to obtain a very good sampling of shorter time-scales, that turned out to be critical in the context of the variability study of our targets. As we were intending to study the variability in line profiles, we focused on high quality spectra with high signal-to-noise ratios, in most cases significantly higher than 200 (see Table 1).

3. The optical spectrum

We plot the mean spectra of our three targets in Figure 1. These spectra are in excellent agreement with the spectral types and luminosity classes reported in the literature (see Section 1). The main absorption and emission lines are labelled in the figure. We note that, in the case of HD 15570, a spectrum covering the whole visible domain is given in De Becker et al. (2006).

When the spectra of our three targets are compared, several common features are worth mentioning:

- the blue spectrum is dominated by the strong, broad, and asymmetric emission of He II λ 4686,
- H α is in strong emission, with a shape similar to that of He II λ 4686,
- the second strongest emission lines in the blue spectrum are N III $\lambda\lambda$ 4634,4641,

Table 2: Journal of the observations for HD 14947, HD 15570 and HD 16691. The heliocentric Julian date is given as HJD - 2 450 000, and the date (yyyy/mm/dd) is that of the beginning of the night. In each case, the spectral domain (blue or red) is specified (available in electronic form only).

	HD 14947			HD 15570			HD 16691		
	HJD	Date	Domain	HJD	Date	Domain	HJD	Date	Domain
1	3286.560	2004/10/07	blue	1811.640	2000/10/23	blue	3286.586	2004/10/07	blue
2	3289.681	2004/10/10	blue	1812.638	2000/10/24	blue	3289.647	2004/10/10	blue
3	3290.624	2004/10/11	blue	1813.670	2000/10/25	blue	3290.581	2004/10/11	blue
4	3296.666	2004/10/17	blue	1814.665	2000/10/26	blue	3295.616	2004/10/16	blue
5	3648.483	2005/10/04	red	1815.666	2000/10/27	blue	3296.624	2004/10/17	blue
6	3648.652	2005/10/04	blue	1819.606	2000/10/01	blue	3648.529	2005/10/04	red
7	3649.454	2005/10/05	red	1821.631	2000/10/03	blue	3648.588	2005/10/04	blue
8	3650.385	2005/10/06	red	2163.604	2001/09/10	blue	3649.641	2005/10/05	red
9	3650.619	2005/10/06	red	2164.635	2001/09/11	blue	3650.567	2005/10/06	red
10	3652.458	2005/10/08	red	2165.609	2001/09/12	blue	3652.374	2005/10/08	red
11	3652.614	2005/10/08	blue	2167.583	2001/09/14	blue	3652.500	2005/10/08	red
12	3653.366	2005/10/09	red	2170.626	2001/09/17	blue	3652.555	2005/10/08	blue
13	3654.378	2005/10/10	red	2518.603	2002/08/31	blue	3653.407	2005/10/09	red
14	3654.433	2005/10/10	blue	2520.545	2002/09/02	blue	3653.460	2005/10/09	blue
15	3654.605	2005/10/10	blue	2523.630	2002/09/05	blue	3654.635	2005/10/10	blue

Table 2: (continued)

16	3982.643	2006/09/03	blue	2524.585	2002/09/06	blue	3980.610	2006/09/01	blue
17	3984.629	2006/09/05	blue	2527.594	2002/09/09	blue	3984.602	2006/09/05	blue
18	4033.468	2006/10/24	blue	2528.602	2002/09/10	blue	4033.436	2006/10/24	blue
19	4033.553	2006/10/24	blue	2529.584	2002/09/11	blue	4033.524	2006/10/24	blue
20	4033.664	2006/10/24	blue	2531.594	2002/09/13	blue	4033.631	2006/10/24	blue
21	4034.383	2006/10/25	blue	2532.593	2002/09/14	blue	4034.437	2006/10/25	blue
22	4034.643	2006/10/25	blue	2533.546	2002/09/15	blue	4034.494	2006/10/25	blue
23	4397.373	2007/10/23	blue	2916.650	2003/10/03	blue	4034.555	2006/10/25	blue
24	4397.432	2007/10/23	blue	2918.595	2003/10/05	blue	4034.614	2006/10/25	blue
25	4397.491	2007/10/23	blue	2919.577	2003/10/06	blue	4397.343	2007/10/23	blue
26	4397.568	2007/10/23	blue	2922.609	2003/10/09	blue	4397.404	2007/10/23	blue
27	4401.342	2007/10/27	blue	2925.620	2003/10/12	blue	4397.461	2007/10/23	blue
28	4401.401	2007/10/27	blue	2928.616	2003/10/15	blue	4397.542	2007/10/23	blue
29	4401.461	2007/10/27	blue	2934.620	2003/10/21	blue	4397.596	2007/10/23	blue
30	4401.543	2007/10/27	blue	3286.612	2004/10/07	blue	4400.412	2007/10/26	blue
31	4402.360	2007/10/28	blue	3287.487	2004/10/08	blue	4400.484	2007/10/26	blue
32	4402.415	2007/10/28	blue	3289.518	2004/10/10	blue	4400.542	2007/10/26	blue
33	4402.470	2007/10/28	blue	3290.510	2004/10/11	blue	4400.595	2007/10/26	blue
34	4402.561	2007/10/28	blue	3294.506	2004/10/15	blue	4402.335	2007/10/28	blue
35	4404.489	2007/10/30	blue	3295.519	2004/10/16	blue	4402.348	2007/10/28	blue
36	4405.371	2007/10/31	blue	3296.509	2004/10/17	blue	4402.442	2007/10/28	blue
37	4405.421	2007/10/31	blue	3648.506	2005/10/04	red	4402.499	2007/10/28	blue

Table 2: (continued)

38	4405.470	2007/10/31	blue	3649.612	2005/10/05	red	4402.534	2007/10/28	blue
39	4405.547	2007/10/31	blue	3650.407	2005/10/06	red	4403.391	2007/10/29	blue
40	4408.364	2007/11/03	blue	3652.478	2005/10/08	red	4403.443	2007/10/29	blue
41	4408.419	2007/11/03	blue	3653.386	2005/10/09	red	4403.494	2007/10/29	blue
42	4408.440	2007/11/03	blue	4400.455	2007/10/26	blue	4403.580	2007/10/29	blue
43	4408.491	2007/11/03	blue	4400.513	2007/10/26	blue	4405.346	2007/10/31	blue
44	4408.569	2007/11/03	blue	4400.570	2007/10/26	blue	4405.395	2007/10/31	blue
45	4409.391	2007/11/04	blue	4400.622	2007/10/26	blue	4405.445	2007/10/31	blue
46	4409.445	2007/11/04	blue	4401.370	2007/10/27	blue	4405.497	2007/10/31	blue
47	4409.550	2007/11/04	blue	4401.430	2007/10/27	blue	4405.522	2007/10/31	blue
48	4409.571	2007/11/04	blue	4401.489	2007/10/27	blue	4405.572	2007/10/31	blue
49	4411.380	2007/11/06	blue	4401.571	2007/10/27	blue	4406.336	2007/11/01	blue
50	4411.449	2007/11/06	blue	4403.418	2007/10/29	blue	4406.452	2007/11/01	blue
51	4411.586	2007/11/06	blue	4403.468	2007/10/29	blue	4406.504	2007/11/01	blue
52	4412.405	2007/11/07	blue	4403.553	2007/10/29	blue	4406.563	2007/11/01	blue
53	4413.405	2007/11/08	blue	4404.401	2007/10/30	blue	4409.363	2007/11/04	blue
54	4413.432	2007/11/08	blue	4404.458	2007/10/30	blue	4409.418	2007/11/04	blue
55	4413.547	2007/11/08	blue	4404.519	2007/10/30	blue	4409.472	2007/11/04	blue
56	4414.484	2007/11/09	blue	4406.363	2007/11/01	blue	4409.502	2007/11/04	blue
57	4414.575	2007/11/09	blue	4406.425	2007/11/01	blue	4409.599	2007/11/04	blue
58	4416.374	2007/11/11	blue	4406.478	2007/11/01	blue	4410.393	2007/11/05	blue
59	4417.554	2007/11/12	blue	4406.532	2007/11/01	blue	4410.449	2007/11/05	blue

Table 2: (continued)

60	4417.579	2007/11/12	blue	4408.392	2007/11/03	blue	4410.500	2007/11/05	blue
61	4419.442	2007/11/14	blue	4408.464	2007/11/03	blue	4410.611	2007/11/05	blue
62	4419.471	2007/11/14	blue	4408.517	2007/11/03	blue	4413.375	2007/11/08	blue
63	4423.374	2007/11/18	blue	4408.542	2007/11/03	blue	4413.509	2007/11/08	blue
64	4423.503	2007/11/18	blue	4410.362	2007/11/05	blue	4416.527	2007/11/11	blue
65				4410.420	2007/11/05	blue	4416.590	2007/11/11	blue
66				4410.528	2007/11/05	blue	4417.437	2007/11/12	blue
67				4410.553	2007/11/05	blue	4417.497	2007/11/12	blue
68				4411.414	2007/11/06	blue	4417.525	2007/11/12	blue
69				4411.500	2007/11/06	blue	4419.519	2007/11/14	blue
70							4423.349	2007/11/18	blue

- the spectral region between about 4600 and 4720 Å presents a broad emission bump,
- $H\beta$ displays a clear P Cygni shape, with an additional very weak emission shoulder on the blue side of the absorption component¹.

Beside these similarities, it should be pointed out that the strong emission lines (He II and $H\alpha$) are significantly stronger in the case of HD 16691, as compared to the two other stars. The N III emission doublet of HD 16691 presents also a rather confused shape with respect to the well individualized ones observed in HD 14947 and HD 15570. In addition, a slightly more complex profile is observed for $H\beta$ for the same star, with a weak additional emission component on the top of the P Cygni profile. The latter feature is not obvious in the mean spectrum shown in Figure 1, but is observed in some profiles presented in Figure 2. The $\text{C III } \lambda\lambda 4647,4650$ and $\text{C IV } \lambda 4660$ features are much less pronounced in the case of HD 16691, but the $\text{N V } \lambda\lambda 4606,4619$ absorption lines are somewhat stronger than in the case of HD 14947 and HD 15570.

4. Results

We first searched for significant line profile variations using the Temporal Variance Spectrum (TVS) technique as described by Fullerton et al. (1996), and previously applied for instance by De Becker & Rauw (2004). This technique was first applied to the complete

¹This weak emission on the blue side of $H\beta$ is most probably a residual from the broad emission component of the P Cygni profile that is not completely compensated by the narrower blue shifted absorption. A broad emission component from the wind is indeed expected, considering the width of other lines originating from the stellar wind such as $\text{He II } \lambda 4686$ and $H\alpha$.

time series. For the three stars, very significant variations are detected mostly in the case of the He II λ 4686, H β and H α lines (at the 99% confidence level). The profiles of these lines, along with the square root of the TVS, are represented for HD 14947, HD 15570 and HD 16691 in Figures 2 and 3. For all stars, the variability level of the He II and H α lines is higher than that of H β (see below for more detailed individual discussions). We insist on the fact that the TVS of H α is computed from a limited number of spectra all collected in October 2005 (see Table 2). In addition, we note that the behaviour of He II λ 4686 and H β presents strong similarities, as illustrated by the variations of the asymmetric profiles in Figure 2.

We used the generalized Fourier technique described by Heck et al. (1985), and revised by Gosset et al. (2001). This technique is especially adapted to the case of unequally spaced data. We systematically applied this technique to our spectral time series, in order to search for possible frequencies (or more specifically the corresponding time-scales) ruling the detected variations. Our approach consisted in computing the power spectrum at each wavelength step leading to a two-dimensioned power spectrum. Mean periodograms were then computed to obtain an overview of the power as a function of frequency for the whole wavelength interval considered in the temporal analysis. We also applied prewhitening techniques considering candidate frequencies in order to check their capability to reproduce the spectral variations (see e.g. De Becker & Rauw 2004, for applications of these techniques to line profile variability analyses). Most of the time, we separately considered the complete data set (about 60 spectra for each star in the blue domain), and the 2007 data set that offers an improved temporal sampling more adequate to search for short term variations (i.e. typically from several hours up to a few days). We note that the detailed temporal analyses were only performed on blue spectra. Our red spectra time series are indeed too limited and too sparse for this purpose.

4.1. HD 14947

Beside the variations in the profile of He II λ 4686 and H β , the TVS analysis revealed also lower amplitude (though significant) variations in N III $\lambda\lambda$ 4634,4641 and in He II λ 4542 (in absorption). We noted also marginal variations in He I λ 4471.

The Fourier technique applied to the complete data set (57 blue spectra) revealed a rather complex mean power spectrum, similar for all lines presenting significant variability. We report on highest peaks located at frequencies of about 0.14, 0.33 and 0.88 d⁻¹ (the latter is likely at least partly an alias of 0.14 d⁻¹), but it is quite difficult to discriminate between them in terms of dominating frequencies. We therefore focused mainly on the 2007 data set (42 blue spectra spread over \sim 26 days), in order to get rid of potential long term trends (physical or not) likely to be present in long time series, and to isolate preferentially shorter time scales. The mean periodogram obtained for He II λ 4686 on the 2007 time series is presented in Figure 4. It was calculated between 4678 and 4694 Å, i.e. the wavelength interval where the variability is the stronger. As we obtained data with time intervals as short as one or two hours between two consecutive spectra, we were able to investigate frequencies as high as 10 d⁻¹. However, as we did not detect any significant power at high frequencies, we limit the discussion to the frequency interval between 0 and 5 d⁻¹. As can be seen in the upper panel of Figure 4, the power spectrum is dominated by a frequency close to 0.139 d⁻¹, corresponding to a time scale of the order of 7.2 d. Prewhitening with the latter frequency leads to a rather good result, as shown in the middle panel of the same figure. However, some residual power is still present. The same analysis performed on the H β line revealed a similar power spectrum, with the highest peak located at a frequency of 0.1425 d⁻¹. In this case, much more residual power remains after prewhitening than in the case of the He II line.

4.2. HD 15570

A significant variability has already been reported in He II λ 4686 Å and H β by De Becker & Rauw (2005). The latter analysis was based on a fraction of the data set discussed in this paper (up to 2004). The main improvement of the present study comes from the significantly better sampling of shorter time-scales thanks to the 28 spectra collected in 2007 (over about 11 days). We do not report on any significant variability for the other lines of the blue spectrum. However, very significant variations are detected for H α , even though our temporal sampling of this line did not allow us to establish the time-scale of these variations. Significant variations of the H α line were already reported by Polcaro et al. (2003).

The power spectrum of the complete time series (64 blue spectra) is dominated by a peak located very close to a frequency of about 1 d^{-1} (and corresponding aliases), most probably related to the sampling frequency of the major part of the time series (mostly before 2007). A second family of peaks is also revealed, with a strongest peak located at a frequency close to 1.37 d^{-1} . Once again, we clarified the situation by considering only the 2007 data set. In this case, the power spectrum is dominated by two components: a poorly constrained long term trend (with essentially its $1 - \nu$ alias)², and a series of peaks at $\nu_i = \nu_o + i$ (ν_o being close to 0.37 d^{-1}), with a highest peak for i equal to 1 and to 2 respectively for H β and He II λ 4686 (along with their aliases at $1 + i - \nu_i$). This situation is illustrated in Figure 5, where the result of successive prewhitening with two frequencies is shown for He II λ 4686 (left part) and H β (right part). Even though we scrupulously selected the highest peaks to prepare Figure 5, it should be noted that we obtain very similar results with frequencies close to 1.37 and 2.37 d^{-1} (corresponding respectively to time scales of

²The frequency close to 0.1 d^{-1} may be related to the timespan of the data collected in 2007, of the order of 11 days.

17.5 and 10.1 h). This is not unexpected as the corresponding peaks have very similar amplitudes. Our temporal sampling seems inadequate to discriminate between these two frequencies. When considering the complete time series, the time scale of about 17.5 h is clearly preferred. However, it should be noted that the power spectrum of the complete time series is strongly affected by non physical peaks (see above) which could bias the relative amplitudes of other peaks. We finally note that the residual power spectra shown in Figure 5 present families of low amplitude peaks at frequencies slightly different from those of the main family reported above.

Considering the rather short time scales reported above, one may wonder whether spectra collected during a same night show clear variations. The TVS technique applied to reduced times series containing 4 spectra spread over maximum 6 hours revealed indeed significant variations for most of the nights where several spectra were obtained. This lends some support to the idea that at least a part of the behaviour of the line profiles of HD 15570 is ruled by a process occurring on time-scales shorter than a day.

4.3. HD 16691

We detect a significant variability in the profiles of all the strongest lines in the blue spectrum, as well as in $H\alpha$. The TVS presents a triple peaked structure, whilst a double peaked structure was observed for the two other stars investigated in our study. The most spectacular variations are observed in the case of $\text{He II } \lambda 4686$ and $H\alpha$. In the case of the $\text{He II } \lambda 4686$ and $H\beta$ lines, the variability reaches its highest level in the red part of the profile. The variations in the profile of these two lines are remarkably correlated. The inspection of the spectra suggests that at least two components are present in this He II line (see individual profiles in Figure 2). However, the asymmetry of the profile remains unchanged all along our time series in the sense that the more intense part of the profile

is always found on the red side. It should be noted that the variations observed in He II λ 4686, H β and H α are very similar to those observed in the case of HD 14947 and HD 15570, but with a much higher amplitude. The investigation of the N III lines at 4634 and 4641 Å strongly suggests that two doublets are present. In order to illustrate this, we have overplotted the N III complex profile observed on HJD 2 453 295.616 (#4 in Table 2) to a synthetic profile made of two shifted pairs of Gaussians superimposed on a broad bump similar to that observed in actual data. The two horizontal lines below the profile in the upper panel of Figure 6 illustrate the wavelength interval between two Gaussians in a given pair. This interval has been fixed at a constant value of about 7 Å in all fits, in agreement with the expected separation between N III lines respectively at 4634 and 4641 Å. The agreement between the observed profile and the synthetic one strongly suggests that two shifted N III doublets are present, or maybe that the two N III lines present a double peaked shape similar to that expected e.g. for a rotating disk.

The power spectrum of the complete time series (64 blue spectra) reveals a dominant peak at a frequency of 0.505 d^{-1} (corresponding to a time scale of 1.98 d) for He II λ 4542, N III λ 4634, N III λ 4641, He II λ 4686 and H β (see Figure 7). We repeated the analysis on the 2007 data set (46 blue spectra) and we obtained periodograms dominated by the same frequency. Prewhitening with this frequency yields excellent results, as can be seen in Figure 7 for the complete data set, except for the N III lines where significant residuals are present in the middle panel³. We note that frequencies close to this one were already

³The residual power is however much lower when the 2007 data set is considered. Because of the large emission bump present between 4600 and 4720 Å, this wavelength interval is quite sensitive to normalization errors. Slight deviations in the level of this emission bump may have an impact on the result of the Fourier analysis by introducing some additional – and not physical – signal in the power spectrum.

detected, though with some ambiguity, using the data set made of spectra from 2004 to 2006 (only 18 spectra). The gathering of more data, mostly with a better sampling of short time-scales, tends to confirm that a stable clock with a period of about 2 d is ruling the strong variability observed in the blue spectrum of HD 16691.

5. Discussion

5.1. Description of the variability

5.1.1. Preliminary summary

Considering the results presented in Section 4, we can formulate a series of remarks about the behaviour of our three sample stars. The various points worth noting can be separated in similarities and differences. First, we consider the following common features in the temporal behaviour of the three stars, in addition to the similarities of the mean spectrum already enumerated in Section 3:

- the main variations are observed for He II λ 4686, H β and H α .
- the variations of He II λ 4686 consist mainly in an alternating amplification and reduction of its asymmetry.
- a similar variation of the profile asymmetry is observed in the absorption component of H β , with a multi-component TVS whose amplitude is stronger on the red side.
- the variations in the profile of He II λ 4686 and H β are correlated, both in time-scale and in morphology (the amplification of the asymmetry occurs at the same time in both lines).

On the other hand, significant differences are found in the behaviour of the spectral lines investigated in this study:

- HD 16691 is clearly the most variable star of our sample, both in the amplitude of the variations and in the ubiquity of its variability. Significant variations are indeed observed in all the prominent lines we investigated in the blue spectrum, and in $H\alpha$. Its TVS presents a central contribution in addition to the two other ones found also in the other stars of our sample.
- HD 14947 presents also some significant variations in the N III emission lines, but the same lines in the spectrum of HD 15570 seem to be quite stable.
- the amplitude of the variations in the asymmetry of the He II λ 4686 and $H\beta$ lines increases from HD 14947 to HD 15570, to HD 16691. The latter one, in its extreme configuration, suggests a partial deblending of two main emission components contributing to the profile.
- the profile of the N III emission lines is rather confused in the case of HD 16691, and can be modelled as consisting of the blending of two pairs of lines.
- in the case of HD 16691, a stable and well-established variability time-scale is determined (~ 2 d). For the other two stars, a significant part of their behaviour appears to be determined by time-scales of about 7.2 d and 17.5 h (or perhaps 10.1 h) respectively for HD 14947 and HD 15570. However, these time-scales do not seem to represent completely the behaviour of their line profiles.

5.1.2. *Multi-Gaussian fittings*

When confronted to a rather complex line profile variability, it may be a good starting point to disentangle the various components likely to contribute to these profiles. From this, the line profile variability may be investigated by varying some of these components in position or in intensity, in order to check what is the impact of this varying component on the line profile.

To perform such a simple morphological description of the line profile (without hydrodynamic or radiative transfer code), we started with the following hypotheses:

- the line profiles can be split into a limited number of Gaussian components,
- the parameters of each individual components can be tuned to reproduce the observed line profiles (absorption, emission, or P Cygni profiles).

In the case of $H\beta$, the P Cygni profile is clearly dominated by its absorption component, except perhaps for HD 16691. In order to produce synthetic profiles similar to those observed for the stars considered in this study, we used a mathematical function such as Equation 1 in De Becker et al. (2006), with the required number of Gaussians. For the P Cygni profile, we used two Gaussians shifted in wavelength with opposite signs. The $H\beta$ profile morphology of HD 14947 and HD 15570 can at first sight be reproduced using a P Cygni component and an additional absorption (or P Cygni with a weak emission component) to reproduce its asymmetry. For HD 16691, there is a clear additional emission component seen on top of the profile in some spectra (see e.g. #32 in the lower right panel of Figure 2). The result of the fit is shown in Figure 8. This set of components fits the morphology of the $H\beta$ line quite well. For the He II line of HD 16691, we fitted the profiles using 4 components: 3 Gaussians of similar widths and intensities representing emission components, and a broad emission component used to account approximately for the presence of the large underlying emission

bump. We note that it was necessary to adapt the normalization factors of two components (by about 10 %, sometimes more) between the two configurations to obtain acceptable fits. The results of these fits are shown in Figure 9. In the case of HD 14947 and HD 15570, we reproduced quite well the profiles using the same approach, but with somewhat lower amplitude spectral shifts of the Gaussians from one spectrum to the other.

A strong contribution of the observed variations can be reproduced to some extent by varying the position of the lateral Gaussians by at most a few tens of km s^{-1} . However, the normalization of the Gaussians had also to be adapted from one spectrum to the other at a level that is sometimes significantly larger than the expected level of variations related to normalization errors in that region of the blue spectrum. We caution however that the observed profiles are only approximately represented with Gaussians. Significant deviations from this simple representation are indeed observed in many spectra.

5.1.3. *Minimum profile analysis*

We built minimum emission spectra for each star by assigning to each spectral resolution element the minimum flux value of the corresponding spectral bin among the spectra of the time series. We then subtracted the minimum He II λ 4686 and H β profiles from each individual observed profile in our time series. The residuals reveal the spectral location where some excess flux is detected in the line, in addition to the minimum profile.

The most striking results are obtained for HD 16691, as illustrated in Figure 10. A large fraction of the He II profiles display double-peaked residuals, suggesting that a variable emitting volume contributes significantly both to the blue and to the red wings of the line, on top of a minimum broad emission. The typical separation between peaks in the residuals is of the order of 500 km s^{-1} , and their position seems to be rather stable in wavelength,

with variations generally of at most $10\text{-}20\text{ km s}^{-1}$ from one observation to the other (see the vertical lines on the left part of Figure 10). However, in the case of some spectra, other excess components with higher amplitudes are also observed (see e.g. the residual #13 in the negative radial velocity part). It is also interesting to note that at several epochs, only the blue part of the line presents a significant excess with respect to the minimum profile. We do not observe such peaks with a striking velocity confinement in the case of $\text{H}\beta$.

HD 14947 and HD 15570 have in common to present the bulk of their excess with respect to the minimum emission profiles generally only on one side of the profile: at null or slightly negative velocities for the He II line, and at null or slightly positive velocities for $\text{H}\beta$ in those examples illustrated in Figures 11 and 12. We note that lower amplitudes excesses are also measured at other radial velocities, but with a much lower amplitude. This agrees with the shape of the TVS plotted in Figure 2 for these two stars. This could indicate that the material that produces an extra (blueshifted) $\text{He II } \lambda 4686$ emission simultaneously produces an extra $\text{H}\beta$ absorption. The main difference between these two stars comes from the fact that the residuals are more peaked and regular in the case of HD 15570. For the latter star, the peak in the residuals of $\text{H}\beta$ seems to be quite stable in wavelength.

5.2. Interpretation

5.2.1. A binary scenario?

Significant line profile variations may be the signature of a binary system. For instance, we mention the case of the very massive binary WR 20a (Rauw et al. 2005) whose $\text{He II } \lambda 4686$ profiles are similar to those observed in the case of the three stars investigated in this study. In order to check the viability of such a scenario, we had a look at absorption lines less likely to be affected by wind emission to search for radial velocity excursions

attributable to an orbital motion⁴. In addition, we also searched for a periodic variation of the width of the line profile, simultaneously with a variation of its depth. As we are dealing with early-type stars, He I lines are rather weak. We will thus focus on the He II line at 4542 Å.

We measured the radial velocities of He II λ 4542 by fitting Gaussians to the line profiles. In the case of HD 14947, we obtain a mean radial velocity for the complete time series of $-32.1 \pm 7.1 \text{ km s}^{-1}$. We performed a Fourier analysis of the radial velocity series and the power spectrum presents several peaks at various frequencies. The highest peak is found at 0.099 d^{-1} (corresponding to a time-scale of about 10.1 d), with an amplitude close to 6 km s^{-1} . Our measurements of the full width at half maximum (FWHM) of the line profile did not reveal any significant trend attributable to a binary motion. The power spectrum computed on the basis of the measurements of the depth of the line is similar to that obtained for the line profile (see Section 4), with the highest peak at about 0.87 d^{-1} .

In the case of HD 15570, the multiplicity study performed by De Becker et al. (2006) did not reveal any significant radial velocity variation. We completed the latter radial velocity analysis by adding the data collected in 2007. The mean radial velocity measured on the He II λ 4542 line is $-47.1 \pm 5.8 \text{ km s}^{-1}$. The Fourier analysis performed on the radial velocities revealed several peaks with amplitudes not higher than 5 km s^{-1} . However, the Fourier analysis performed on the line depth measurements led to a power spectrum dominated by two peaks respectively at 0.369 and 1.361 d^{-1} , with very similar amplitudes (the first one being the highest). These frequencies belong obviously to the family of frequencies already pointed out in Section 4.2 for this star. We did not obtain any significant result for the FWHM measurements.

⁴We note that the rest wavelengths used to determine the radial velocities were taken from Conti et al. (1977).

Finally, we repeated the same analysis for HD 16691. The mean radial velocity is $-49.6 \pm 9.1 \text{ km s}^{-1}$. None of the three quantities measured on this line presents a large amplitude variability with the same time-scale as reported in Section 4 for the line profiles. However, the peculiar shape of the N III emission profile deserves some attention. The fact that obvious double lines are found for this profile raises the question of the multiplicity of HD 16691. A careful inspection of the line profiles reveals that the spectral position of the components constituting the profile undergoes significant shifts, but with a rather weak semi-amplitude similar to that reported for He II λ 4542, e.g. of the order of 10 km s^{-1} . We fitted every N III emission profile of the complete time series in order to disentangle the four components using the same approach as shown in the left panel of Figure 6. It should be noted that the line intensities do not seem to be constant from one spectrum to the other. This could be due either to intrinsic changes of the components that make up the N III lines⁵ or to changes of the underlying broad emission bump. The derived radial velocities of the Gaussian pairs are respectively of the order of -140 and 70 km s^{-1} . The phase coverage of the time series is rather good, provided the period is 1.98 d (see the results of the line profile temporal analysis in Sect. 4.3), and none of the profiles of our times series shows completely merged components representative of intermediate radial velocities. The four individual components of the N III multiplet undergo only weak velocity shifts, i.e. at most 10 km s^{-1} in semi-amplitude. The behaviour described in Section 5.1.3, with the double-peak shape of the residuals on top of the minimum profile of the He II λ 4686 line, is similar to that of the pair of N III doublets. This situation is difficult to reconcile with the orbital motion of at least two emission components associated to two stars in a binary system. We emphasize

⁵It should be noted that significant changes in the normalization parameters of the components used to reproduce the He II and H β profiles were also requested to fit the profiles with Gaussians from one spectrum to the other.

also that no obvious signature of the presence of a companion has been found in other lines. We therefore cannot report on any signature of binarity for HD 16691.

5.2.2. A single star scenario?

A plausible origin for the variations may be the stellar wind itself. Stellar winds are unlikely spherical and homogeneous. Any large scale structure in the wind may be responsible for additional emission or absorption components in spectral lines produced predominantly in the wind (e.g. He II λ 4686 and H α), or at least partly produced in the wind (e.g. H β). In this context, the strong correlation in the behaviour of the lines investigated in this study may be explained by their common physical origin, i.e. the same structured stellar wind.

None of the three stars present any strong evidence for binarity. Therefore, we consider a phenomenon related to a structured stellar wind, with a variability time-scale possibly related to the stellar rotation (e.g. De Becker & Rauw 2004). Such a phenomenon has been investigated from the theoretical point of view, e.g. corotating interaction regions (see e.g. Cranmer & Owocki 1996; Lobel & Blomme 2008) or a magnetically channelled wind scenario (see e.g. Ud-Doula et al. 2008).

The processes responsible for the formation of spectral lines in stellar atmospheres (stationnary or expanding) are intimately dependent on the density of their production region. Any large scale structure (with a significant density contrast with respect to the surrounding mean wind) will therefore contribute to emission lines (additional contributions due to the enhanced local density), and will have an impact on absorption lines as well (for instance, photospheric light undergoing additional absorption when crossing higher density regions). According to the density contrast and distribution, and to their physical ex-

tension, the morphological impact of such structures on spectral lines may vary substantially.

Large Scale Corotating Structures (LSCS) can be responsible for a substantial line profile variability. On the one hand, any deviation from the axial symmetry of the rotating emitting region will lead to periodic variations ruled by the rotation period. Such features may come from azimuthal inhomogeneities in the mass loss, or from the interaction of the wind plasma with an inclined magnetic field (the so-called *oblique magnetic rotator*). In this context, it is especially worth mentioning recent advances in the modelling of rigidly rotating magnetospheres (Townsend & Owocki 2005; Townsend et al. 2007), with emphasis on the excellent results obtained in the representation of the H α variations in the Bp star σ Ori E (Townsend et al. 2005). On the other hand, smaller scale heterogeneities in the stellar wind are likely to induce additional – not necessarily periodic – variations superimposed on those due to the LSCS. We note that we do not expect small scale density structures distributed across the whole stellar wind (i.e. clumps) to be responsible for the variations reported in this study. Such a wind clumping would more probably yield a uniform TVS, in contradicton with the structured one presented in Figure 2. In addition, clumping is expected to lead to line profile variations with an amplitude of a few per cent at most (e.g. Eversberg et al. 1998), much lower than those described in this paper.

It should be worth checking whether the time-scales found in Sect. 4 are compatible with the putative rotation period of the star. To do so, we used the relations (1 to 3) used by De Becker & Rauw (2004) and the parameters given in Table 3, in order to estimate the expected minimum (constrained by the critical rotation velocity) and maximum (constrained by the projected rotational velocity) rotation periods for the three stars. The results (P_{min} and P_{max}) are quoted in Table 3. In the case of HD 16691 whose variability time-scale seems rather well-established, the 1.98 d time-scale is compatible with the

rotation period. Actually, it is rather close to the critical period below which the star would break up. On the contrary, the time-scale of 7.2 d reported for HD 14947 is closer to the upper limit given in Table 3. The case of HD 15570 is more problematic, in the sense that the reported variability time-scales (17.5 h, or even 10.1 h) are significantly shorter than the break-up rotation period. However, the observed variability time scale may be only a fraction of the actual rotation period if the symmetry of the LSCS is not rigorously cylindrical (e.g. elongated large-scale structure), or if several structures in corotation are present (e.g. structures related to several ‘bright’ or ‘dark’ spots on the stellar surface).

In a scenario where the LSCS is confined by a simple, bipolar, stellar magnetic field, the apparent extension of the structure responsible for the bulk of the emission of He II λ 4686 can be converted into a raw approximation of the intensity of the required magnetic field. Considering that the structure cannot be stabilized by the magnetic field beyond the Alfvén radius (i.e. the radius where the kinetic and magnetic energy densities equilibrate), we obtain the following relation:

$$B_*^2 = \frac{\mu_o}{4\pi} \frac{\dot{M} v_\infty}{R_*^2} \left[\frac{r}{R_*} \right]^4 \left[1 - \frac{R_*}{r} \right]^\beta$$

where we have assumed a radial dependence of the magnetic field (B) of the type $B = B_* (R_*/r)^3$. In this equation, B_* is the stellar magnetic field strength at the equator, B is the magnetic field strength at a distance r from the center of the star, v_∞ is the terminal velocity, \dot{M} is the mass loss rate, μ_o is the permeability of free space, and β is the index of the velocity law. We used a β equal to 1. Considering that the extension of the corotating structure of HD 16691 is of the order of 250 km s^{-1} in radial velocity space (on the basis of the central position of the two lateral Gaussians in Section 5.1.2) and using the quantities given in Table 3, we obtain a stellar magnetic field strength of about 130 G. If we rather consider that the Alfvén radius corresponds to the maximum extension of the variable part of the profile (i.e. about 500 km s^{-1} , corresponding also to the radial velocity separation

Table 3: Stellar parameters of HD 14947, HD 15570 and HD 16691, and estimated minimum and maximum rotation periods. The references for the stellar parameters are: (a) Martins et al. (2005), (b) Penny (1996), (c) Conti & Ebbets (1977), (d) Markova et al. (2005), (e) Leitherer (1988) and (f) Herrero et al. (2000).

	HD 14947	HD 15570	HD 16691
Sp. Type	O5If ⁺	O4If ⁺	O4If ⁺
M_* (M_\odot) ^(a)	51	58	58
R_* (R_\odot) ^(a)	19.5	18.9	18.9
L_* (L_\odot) ^(a)	7.4×10^5	8.7×10^5	8.7×10^5
$V_{rot} \sin i$ (km s^{-1})	133 ^(b)	130 ^(c)	150 ^(c)
V_∞ (km s^{-1})	2300 ^(d)	2700 ^(e)	2300 ^(d)
\dot{M} ($M_\odot \text{ yr}^{-1}$)	$1.52 \times 10^{-5(d)}$	$1.78 \times 10^{-5(f)}$	$1.25 \times 10^{-5(d)}$
P_{min} (d)	1.8	1.6	1.6
P_{max} (d)	7.4	7.4	6.4

between the peaks in the residuals in Figure 10), we derive a magnetic field strength of about 250 G. For HD 14947 and HD 15570, the narrower variable region of the He II profile leads to somewhat lower B values. At this level of approximation, and in the context of a magnetically confined LSCS, we consider that a stellar magnetic field with a strength of a few 100 G is compatible with our observations.

On the basis of the above discussion, a single star scenario may provide a valuable interpretation for the spectral behaviour described in the previous sections.

5.2.3. *A common interpretation?*

As mentioned earlier in this study, several similarities are observed in the spectrum and in the temporal behaviour of the three stars we investigated. The idea of a common scenario is therefore worth considering. The differences between the lines of HD 16691 and those of the two other stars (except for N III) are more quantitative than qualitative (i.e. similar behaviour but different amplitudes). Provided the three stars are single, we may envisage an LSCS scenario where the quantitative differences may be explained (i) by various dimensions of the large scale structure and (ii) by different inclinations of the corotating structure with respect to the line of sight, leading to different radial velocity shifts of individual emitting regions contributing to line profiles.

In all cases, a line such as He II λ 4686 is expected to be produced by the mean wind, with substantial additional emission from the LSCS. The latter emission may appear as a double peak, in a way similar to that of a corotating emission region (see for instance Oef stars: ζ Pup, BD +60° 2522, λ Cep, HD 192281, HD 14442, HD 14434). The double peaked emission plus that of the mean wind can explain the complexity of the He II λ 4686 profile. For H β , the main part of the profile is a classical P Cygni component. However, the

careful inspection of the $H\beta$ line profiles revealed the presence of an additional absorption component moving simultaneously with at least one component of the $\text{He II } \lambda 4686$ profile. This additional absorption may be due to the higher opacity of the LSCS at some phases of the rotation cycle. The additional small emission observed in the case of HD 16691 may also come from the LSCS. To some extent, the slight asymmetries reported in the case of $\text{He II } \lambda 4542$ may also be explained by the additional absorption due to the LSCS. This common origin is able to explain the strong correlation between the asymmetries of the $\text{He II } \lambda 4686$ and $H\beta$ lines, as clearly shown in Figure 2. The increasing amplitude of these asymmetries from HD 14947 to HD 16691 may be a result of the combined effect of different inclinations with respect to the line of sight and of the spatial extension of the LSCS, resulting in the different extensions in the radial velocity space. The two N III doublets observed in the case of HD 16691 suggest that these lines are mostly produced in the LSCS, in a confined emission region. This would imply that the region where the temperature conditions are more favorable for the production of the $\text{N III } \lambda\lambda 4634,4641$ is coincident with the location of the LSCS. The fact that such a feature is not observed for HD 14947 and HD 15570 may at least partly be explained by a lack of coincidence of the production region of the N III lines and of the LSCS. We should not reject a scenario where the LSCS is located at somewhat larger radial distances than the N III emission region in the case of HD 14947 and HD 15570 (explaining the single line shape and the lack of substantial variability), whereas in the case of HD 16691 the LSCS may be extended up to much shorter distances from the star, including almost completely the N III emission region. The location and extension of the LSCS are indeed expected to depend intimately on several parameters such as wind properties and putative magnetic properties of the stars, provided the existence of the LSCS is of magnetohydrodynamic origin. In such a scenario, the variations reported on the intensity of the components contributing to line profiles ($\text{He II } \lambda 4686$, $H\beta$ or $\text{N III } \lambda\lambda 4634,4641$) may be the signature of small asymmetries in the density distribution

of the LSCS. The slight variations in position measured mainly for the N III individual components, and for the residual emission in excess to the minimum profile of He II λ 4686, point also to slight deviations from any cylindrical symmetry for the density distribution in the stellar wind. A large scale structure in the stellar wind modulated by the rotation of the star is therefore likely to explain most of the features observed for the three stars.

6. Conclusions

We presented the very first detailed investigation of the line profile variability of a sample of Of⁺ supergiants, using unprecedented spectral time series mostly in the blue domain. We report on significant correlated variations in the profile of He II λ 4686 and H β .

The stronger variations are found in the spectrum of HD 16691 which presents some peculiarities with respect to HD 14947 and HD 15570. The most striking feature is the N III doublet at 4634,4641 Å, where each line seems to be double with a separation of the order of 200 km s⁻¹. The latter feature is unlikely to be related to a binary scenario. Our temporal analysis points to a period of about 2 d for HD 16691, but the variability time-scale is not so well established for HD 14947 and HD 15570.

When put together, most of the features of the spectral behaviour of the three stars investigated in this study are compatible with a common scenario, with differences that are more quantitative than qualitative. No convincing evidence for the presence of a companion exists for the three targets, rejecting therefore variations related to binarity and colliding-wind phenomena. The behaviour described in the present study is much more compatible with a single star scenario where Large Scale Corotating Structures (LSCS) in the wind contribute significantly to emission and absorption features. Such a scenario appears to be well-suited for the line profile variations of He II λ 4686 and H β (and also

$H\alpha$, even though it has not been investigated in detail in this study). In the context of this scenario, the peculiar shape of the N III $\lambda\lambda$ 4634,4641 profile in HD 16691 is tentatively explained by a coincidence of the region that is most favorable to the production of the N III lines with a particularly extended (in radial velocity space) LSCS. The absence of such a peculiarity for the two other stars is then explained by the lack of such a coincidence.

The single star nature of the three stars investigated in this study, combined with the structured corotating wind scenario, should not be considered as a firm conclusion based on strong observational evidence, but should be rather viewed as the best working hypothesis to date for future investigations of line profile variations of early-type stars, and in particular of Of⁺ supergiants.

MD wishes to express his gratitude to Dr. Eric Gosset for stimulating discussions. The travels to OHP were supported by the Ministère de l'Enseignement Supérieur et de la Recherche de la Communauté Française. This research is also supported in part through the PRODEX XMM/Integral contract, and more recently by a contract by the Communauté Française de Belgique (Actions de Recherche Concertées) – Académie Wallonie-Europe. We would like to thank the staff of the Observatoire de Haute Provence (France) for the technical support during the various observing runs. The SIMBAD database has been consulted for the bibliography.

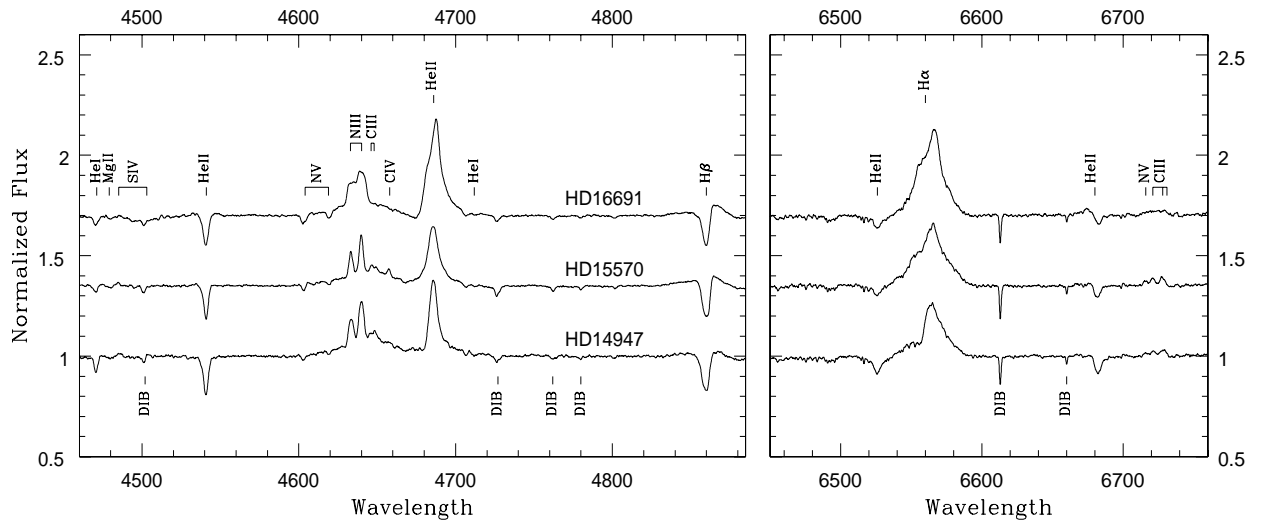


Fig. 1.— Mean visible spectra of HD 14947, HD 15570 and HD 16691 between 4460 and 4890 Å (left part) and between 6450 and 6760 Å (right part).

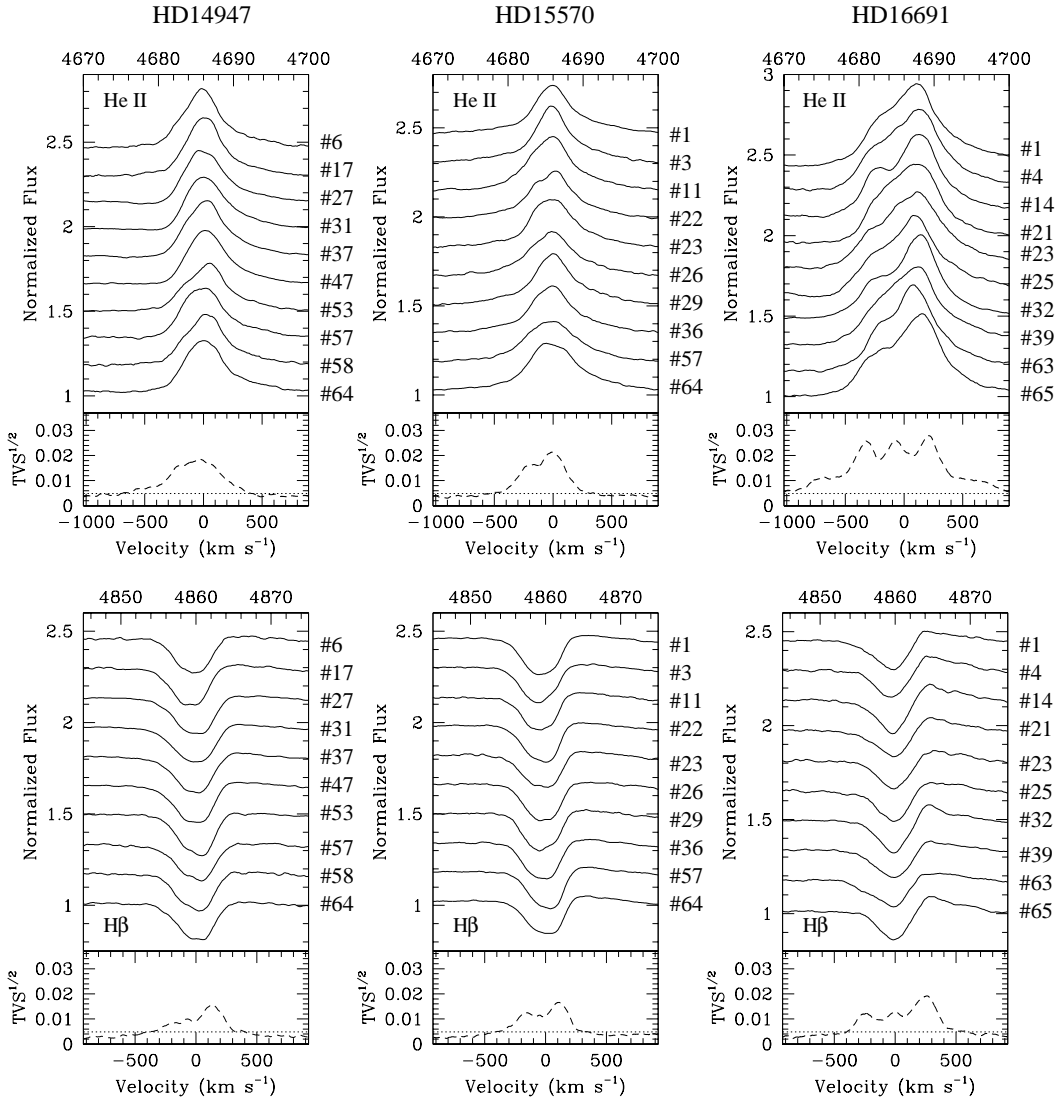


Fig. 2.— Profile variability of the strongest lines respectively for HD 14947, HD 15570 and HD 16691 (from the left to the right). *Upper panels:* He II λ 4686. *Lower panels:* H β . In each case, the upper plot shows a sample of profiles, and the lower one provides the TVS for the complete time series. The numbers on the left of the individual profiles correspond to those attributed in Table 2. The horizontal dotted line in the lower panels stands for the 99% confidence level. In order to give an idea of the relative variability level of every line of each star, the TVS scale is the same in all panels.

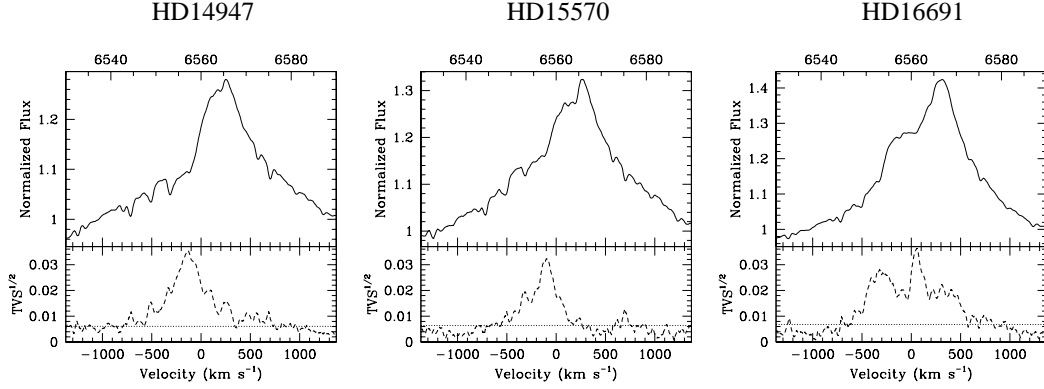


Fig. 3.— Profile variability of the $H\alpha$ line respectively for HD 14947, HD 15570 and HD 16691 (from the left to the right). In each case, the upper plot shows the mean profile, and the lower one provides the TVS for the October 2005 time series in the red domain.

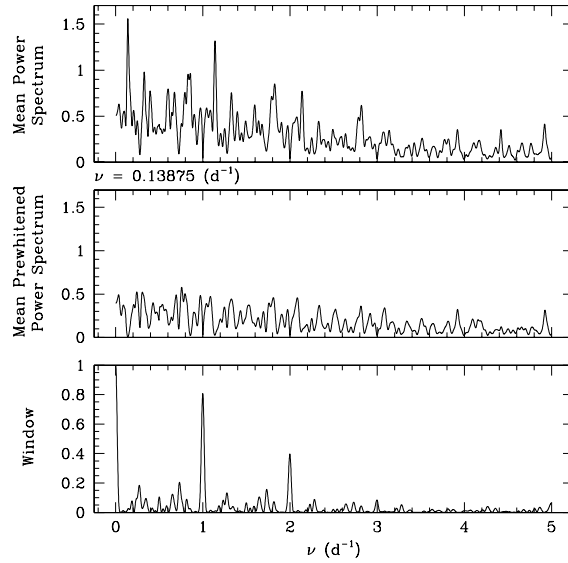


Fig. 4.— Fourier analysis of the $He\ II \lambda 4686$ line between 4678 and 4694 \AA in the case of HD 14947. *Upper panel:* mean power spectrum between 0 and 5 d^{-1} . *Middle panel:* mean power spectrum obtained after prewhitening using the frequency of the highest peak of the initial power spectrum, i.e. 0.13875 d^{-1} . *Lower panel:* spectral window directly related to the sampling of the time series.

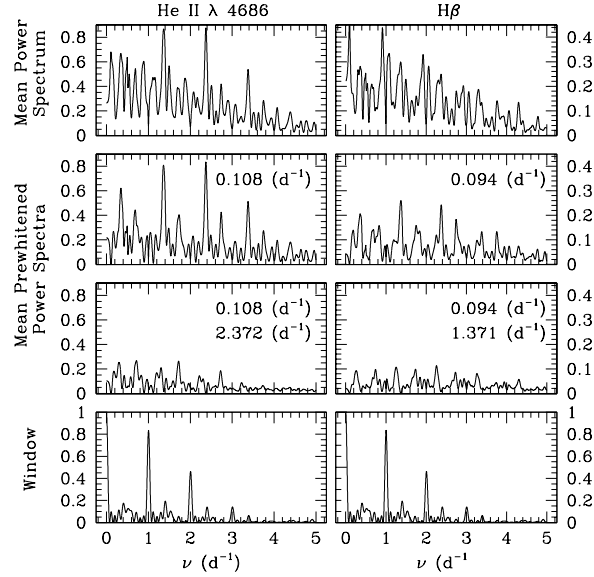


Fig. 5.— Fourier analysis of the He II λ 4686 line between 4678 and 4694 Å (left part) and of H β between 4854 and 4866 Å (right part) in the case of HD 15570. *Upper panel:* mean power spectra between 0 and 5 d⁻¹. *Middle panels:* mean power spectrum obtained after prewhitening using the frequencies specified in each panel. *Lower panel:* spectral window directly related to the sampling of the time series, identical for both lines as it comes from the same times series.

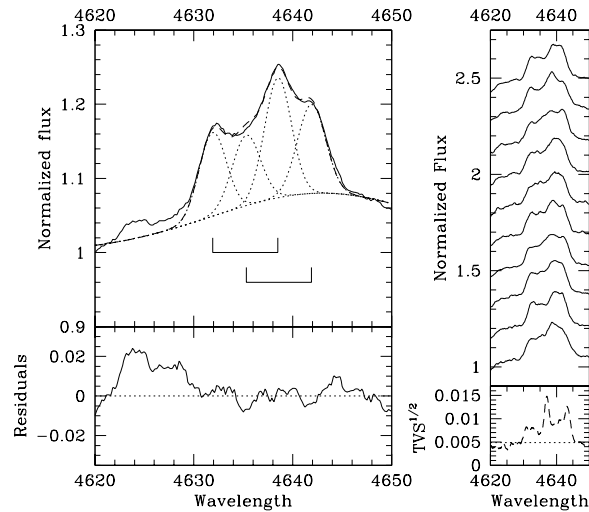


Fig. 6.— N III line profile at 4634,4641 Å in the spectrum of HD 16691. *Left part:* fit of the profile (spectrum #4 in Table 2) using two pairs of Gaussians. The central positions of the four Gaussians correspond respectively to radial velocities of -136.5 , 83.4 , -147.3 and 72.3 km s^{-1} . The lower panel gives the residual of the fit, in the sense data minus model. An additional broad component is used in order to model the emission bump already mentioned in Section 3. *Right part:* variations in the N III line profile illustrated by a sample of spectra (the same as in Figure 2), and by the TVS of the complete time series in the lower panel.

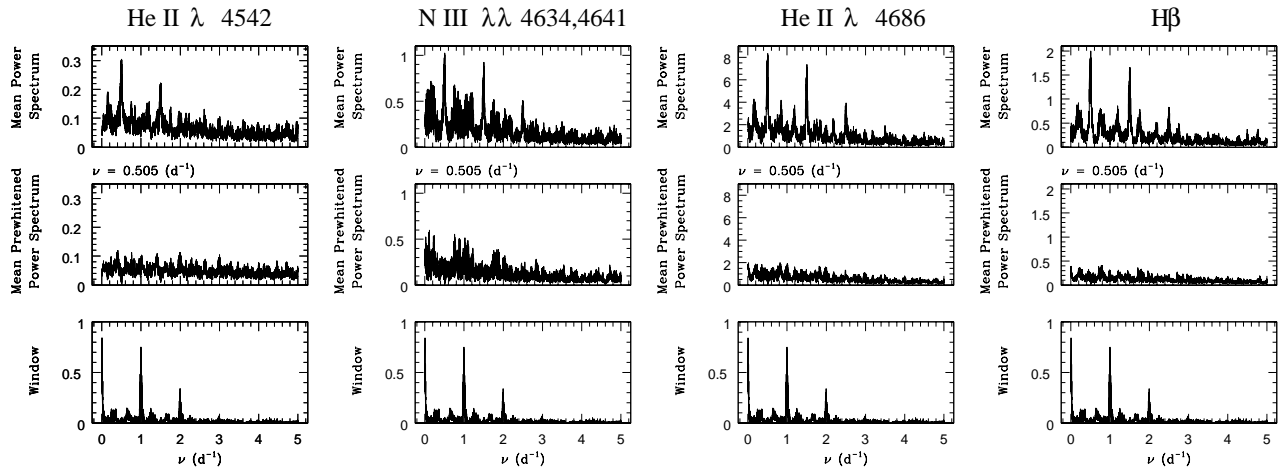


Fig. 7.— Fourier analysis of the complete time series of HD 16691. From the left to the right, the lines investigated are He II λ 4542, N III $\lambda\lambda$ 4634,4641, He II λ 4686 and H β . In each case, the meaning of the three panels is the same as described in Fig. 4. The width of the peak at 0.505 d^{-1} is somewhat larger than that of the peaks found in the spectral window, because it is blended with that of the $1 - \nu$ alias.

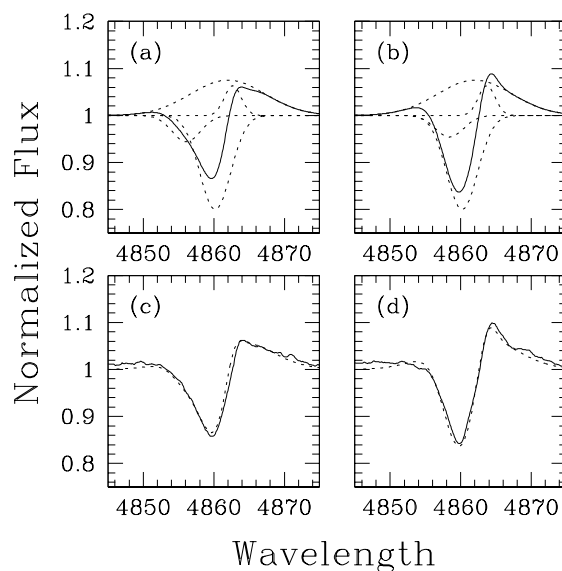


Fig. 8.— Multi-Gaussian fitting of the $H\beta$ profile of HD 16691 at two different epochs (spectra #1 and #32 in Table 2). *Panel (a)*: Synthetic profile with its individual components plotted as dashed lines for spectrum #1. *Panel (b)*: same as panel (a) but for spectrum #32. *Panel (c)*: spectrum #1 with the synthetic profile overplotted. *Panel (d)*: same as panel (c) but for spectrum #32. The wavelengths are expressed in \AA .

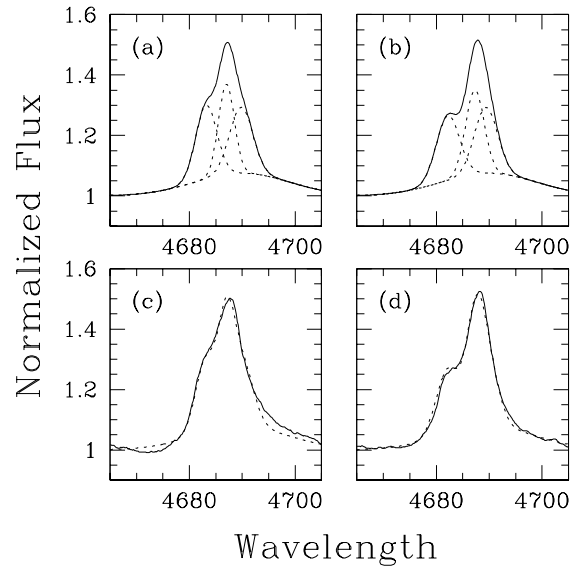


Fig. 9.— Same as Figure 8, but for He II λ 4686.

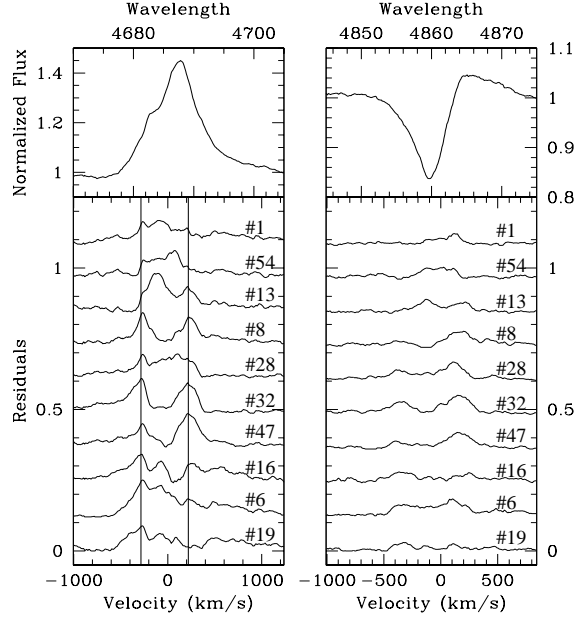


Fig. 10.— *Upper panels:* minimum profiles of He II λ 4686 (*left*) and H β (*right*) of HD 16691 as a function of wavelength expressed in \AA . *Lower panels:* residuals for a sample a 10 spectra of the time series selected in order to cover rather homogeneously the phases between 0 and 1, considering a time-scale of 1.98 d and a T_o corresponding to the time at mid-exposure of the first observation of the series. Residuals have been shifted vertically by a quantity of 0.12 units for the sake of clarity. The bottom scales corresponds to velocities expressed in km s^{-1} . The number of the spectrum as defined in Table 2 is provided in each case. From the top to the bottom, these spectra correspond respectively to the arbitrary phases 0.00, 0.10, 0.20, 0.27, 0.45, 0.50, 0.59, 0.69, 0.81 and 0.93. In the case of He II, the two vertical lines (respectively at -280 and 220 km s^{-1}) emphasize the alignment of the peaks observed in the residuals of most of the profiles.

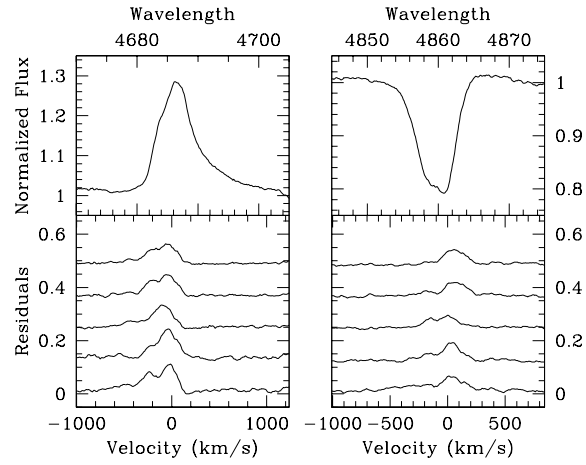


Fig. 11.— Same as Figure 10, but for HD 14947. The five profiles whose residuals are plotted correspond to spectra number #1 to #5, from the top to the bottom.

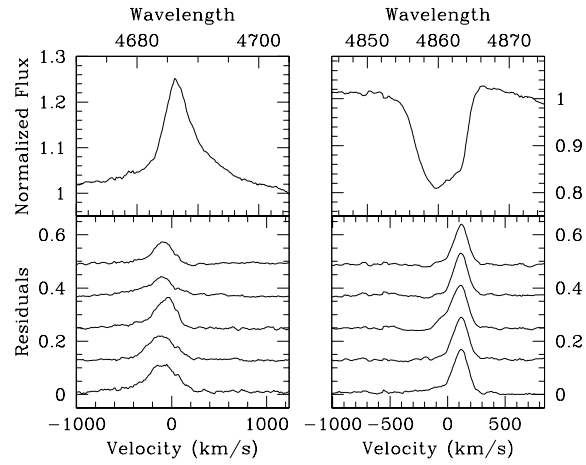


Fig. 12.— Same as Figure 11, but for HD 15570.

REFERENCES

- Cappa, C. E., & Herbstmeier, U. 2000, *AJ*, 120, 1963
- Conti, P. S. 1976, *Memoires of the Societe Royale des Sciences de Liege*, 9, 193
- Conti, P. S., & Ebbets, D. 1977, *ApJ*, 213, 438
- Conti, P. S., Hanson, M. M., Morris, P. W., Willis, A. J., & Fossey, S. J. 1995, *ApJ*, 445, L35
- Conti, P. S., Leep, E. M., & Lorre, J. J. 1977, *ApJ*, 214, 759
- Cranmer, S. R., & Owocki, S. P. 1996, *ApJ*, 462, 469
- De Becker, M., & Rauw, G. 2004, *A&A*, 427, 995
- De Becker, M., & Rauw, G. 2005, in *Massive Stars and High-Energy Emission in OB Associations*, 111–114
- De Becker, M., Rauw, G., & Manfroid, J. 2004, *A&A*, 424, L39
- De Becker, M., Rauw, G., Manfroid, J., & Eenens, P. 2006, *A&A*, 456, 1121
- Eversberg, T., Lepine, S., & Moffat, A. F. J. 1998, *ApJ*, 494, 799
- Fullerton, A. W., Gies, D. R., & Bolton, C. T. 1996, *ApJS*, 103, 475
- Gillet, D., et al. 1994, *A&AS*, 108, 181
- Gosset, E., Royer, P., Rauw, G., Manfroid, J., & Vreux, J.-M. 2001, *MNRAS*, 327, 435
- Heck, A., Manfroid, J., & Mersch, G. 1985, *A&AS*, 59, 63
- Herrero, A., Puls, J., & Villamariz, M. R. 2000, *A&A*, 354, 193

- Leitherer, C. 1988, *ApJ*, 326, 356
- Lobel, A., & Blomme, R. 2008, *ApJ*, 678, 408
- Markova, N., Puls, J., Scuderi, S., & Markov, H. 2005, *A&A*, 440, 1133
- Martins, F., Schaerer, D., & Hillier, D. J. 2005, *A&A*, 436, 1049
- Penny, L. R. 1996, *ApJ*, 463, 737
- Polcaro, V. F., Viotti, R. F., Norci, L., Rossi, C., Eenens, P. R. J., & Corral, L. J. 2003, in *IAU Symposium, Vol. 212, A Massive Star Odyssey: From Main Sequence to Supernova*, ed. K. van der Hucht, A. Herrero, & C. Esteban, 224–+
- Rauw, G., et al. 2005, *A&A*, 432, 985
- Rauw, G., & De Becker, M. 2004, *A&A*, 421, 693
- Townsend, R. H. D., & Owocki, S. P. 2005, *MNRAS*, 357, 251
- Townsend, R. H. D., Owocki, S. P., & Groote, D. 2005, *ApJ*, 630, L81
- Townsend, R. H. D., Owocki, S. P., & Ud-Doula, A. 2007, *MNRAS*, 382, 139
- Ud-Doula, A., Owocki, S. P., & Townsend, R. H. D. 2008, *MNRAS*, 385, 97
- Willis, A. J., & Stickland, D. J. 1980, *MNRAS*, 190, 27P